1 Title: Dynamics and quantitative contribution of the aminoglycoside 6′-*N*-
2 acetyltransferase type Ib [AAC(6′)-Ib] to amikacin resistance

3 Authors: Ophélie d'Udekem d'Acoz[1], Fong Hue[2], Tianyi Ye[1], Louise Wang[1], Maxime
4 Leroux[1], Lucila Rajngewerc[2], Maria S. Ramirez[2], Walter Reisner[3], Marcelo E. Tolmasky[2]
5 and Rodrigo Reyes-Lamothe[1]

6 Affiliations: [1] Department of Biology, McGill University, 3649 Sir William Osler, Montréal,
7 Québec, H3G 0B1, Canada

8 [2] Center for Applied Biotechnology Studies, Department of Biological Science, California
9 State University Fullerton, Fullerton, California

10 [3] Department of Physics, McGill University, 3600 rue université, Montréal, Québec, H3A
11 2T8, Canada

12 Correspondence: rodrigo.reyes@mcgill.ca; mtolmasky@fullerton.edu

13 Running title: AAC(6′)-Ib impact per molecule on amikacin resistance

14
15

Abstract

Aminoglycosides are essential components in the available armamentarium to treat bacterial infections. The surge and rapid dissemination of resistance genes strongly reduce their efficiency, compromising public health. Among the multitude of modifying enzymes that confer resistance to aminoglycosides, the aminoglycoside acetyltransferase AAC(6′)-Ib is the most prevalent and relevant in the clinical setting as it can inactivate numerous aminoglycosides, such as amikacin. Although the mechanism of action, structure, and biochemical properties of the AAC(6′)-Ib protein have been extensively studied, the contribution of the intracellular milieu to its activity remains unclear. In this work, we combined a fluorescent-based system with CRISPR interference method to modulate and quantify the number of AAC(6′)-Ib per cell in *Escherichia coli*. These tools were then used to correlate enzyme concentrations with amikacin resistance levels. Our results show that resistance to amikacin increases linearly with a higher concentration of AAC(6′)-Ib until it reaches a plateau at a specific protein concentration. *In vivo* imaging of this protein shows that it diffuses freely within the cytoplasm of the cell, but it tends to form inclusion bodies at higher concentrations in rich culture media. Addition of a chelating agent completely dissolves these aggregates and partially prevents the plateau in the resistance level, suggesting that AAC(6′)-Ib aggregation lowers resistance to amikacin. These results provide the first step in understanding the cellular impact of each AAC(6′)-Ib molecule on aminoglycoside resistance. They also highlight the importance of studying its dynamic behavior within the cell.

Importance

Antibiotic resistance is a growing threat to human health. Understanding the mechanisms of antibiotic resistance can serve as foundation for developing innovative treatment strategies to counter this threat. While numerous studies clarified the genetics and dissemination of resistance genes and explored biochemical and structural features of resistance enzymes, their molecular dynamics and individual contribution to resistance within the cellular context remain unknown. Here, we examined this relationship modulating expression levels of AAC(6′)-Ib, an enzyme of clinical relevance. We show a linear correlation between copy number of the enzyme per cell and amikacin resistance levels up to a threshold where resistance plateaus. We propose that at concentrations below the threshold, the enzyme diffuses freely in the cytoplasm but aggregates at the cell poles at concentrations over the threshold. This research opens promising avenues for studying enzyme solubility's impact on resistance, creating opportunities for future approaches to counter resistance.

Introduction

The emergence and rapid dissemination of antibiotic resistance genes are among the biggest threats to global health (1, 2). Infections caused by antibiotic-resistant bacteria are rising in hospital and community settings. This growing trend is undermining treatment options and posing a significant risk to the success of medical and dental procedures that rely on preventing bacterial contamination (1). The current number of fatal infections due to resistance is estimated at hundreds of thousands per year, and the number could grow in the future (2). New drugs are urgently needed, but despite calls for action by diverse world organizations, the number of potential new drug candidates remains critically low (1-3). Two major therapeutic strategies have been proposed to deal with this crisis: (1) designing new antibiotics or (2) inhibitors of resistance that can be combined with existing antimicrobials (4). The success of these novel therapies depends on a detailed understanding of the different cellular and molecular mechanisms by which bacteria resist antibiotics (4).

Aminoglycosides are broad-spectrum antibiotics that interfere with normal protein synthesis by binding to the 16S rRNA. While not all classes of aminoglycosides bind to identical sites of the 16S rRNA, in all cases the A site (the ribosome's decoding center) undergoes a conformational change to one resembling the closed state, formed after interacting with the cognate tRNA and mRNA (5). Consequently, the proofreading capabilities of the ribosome are reduced or eliminated, resulting in high levels of mistranslation (6, 7). However, despite the remarkable advances in understanding the mechanism of action of aminoglycosides, there is still much to learn about the nature of

73 the translation errors generated by these drugs (8). Aminoglycosides have become less
74 popular after being broadly utilized for decades due to increased resistance and relatively
75 high toxicity. However, the requirement for effective medications and the need to develop
76 less harmful semisynthetic variations to overcome the most prevalent resistance
77 mechanisms have revitalized interest in their use (9, 10).

78 Amikacin, the most successful semisynthetic aminoglycoside (11), is refractory to
79 most aminoglycoside modifying enzymes, which through acetylation, phosphorylation, or
80 nucleotidylation, are the most common causes of resistance in clinical settings.
81 Unfortunately, amikacin is a substrate for aminoglycoside 6′-*N*-acetyltransferase type I
82 enzymes [AAC(6′)-I], which promote inactivation through acetylation at the 6' amine group
83 of the antibiotic (7, 11). Among *aac(6')-I* genes, *aac(6')-Ib* is the most clinically relevant,
84 being found in the vast majority of multiple aminoglycoside-resistant Gram-negative
85 isolates (12). The *aac(6')-Ib* gene is located within plasmids and chromosomes as part of
86 integrons, transposons, genomic islands, and other genetic structures that facilitate its
87 dissemination at the molecular and cellular level, reaching virtually all Gram-negative
88 bacteria (13). While considerable advances have been made in the understanding of the
89 dissemination mechanisms of *aac(6')-Ib* (7, 14, 15), structural characteristics of the
90 enzyme (16, 17), and its specificity properties (13, 18-20), multiple other aspects remain
91 to be elucidated.

92 A significant gap in our understanding of how AAC(6′)-Ib mediates resistance is its
93 intracellular dynamics. Previous studies have demonstrated that gene amplification is
94 correlated with higher expression of aminoglycoside modifying enzymes and increased
95 resistance levels (21-27). However, these studies rely on the number of gene copies

96 rather than the correlation between the measured number of protein molecules and
97 resistance levels. In this work, we describe the design of a fluorescence-based method
98 to accurately determine the number of molecules of AAC(6′)-Ib and a CRIPSPR
99 interference (CRISPRi) system to regulate the number of AAC(6′)-Ib molecules
100 synthesized. We observed a correlation between the quantity of AAC(6′)-Ib molecules and
101 amikacin resistance up to a threshold where adding additional AAC(6′)-Ib molecules
102 ceases to be associated with increased resistance. Live cell imaging showed that
103 AAC(6′)-Ib aggregates at the poles at higher concentrations, a process that may denature
104 and inactivate the excess molecules. Single molecule microscopy of the dynamics of
105 AAC(6′)-Ib in the cellular context showed that the enzyme freely diffuses in the cytoplasm,
106 not binding to any particular cellular structure. Our results provide a quantitative
107 understanding of the relationship between the number of enzyme molecules and
108 resistance levels. Furthermore, our findings suggest that the upper limit to amikacin
109 resistance arises due to protein aggregation at increased intracellular concentration.

110

111 ## Results

112 ### Mutant gRNAs mediate progressive regulation of AAC(6′)-Ib gene expression

113 To fine-tune AAC(6′)-Ib expression levels, we used CRISPRi. This method relies on a
114 catalytically dead variant of Cas9 (dCas9) that binds a specific DNA sequence but fails to
115 cleave it, producing a roadblock for transcriptional initiation or elongation (28). The level
116 of repression of *aac(6')-Ib* expression is maximum if the guide RNA (gRNA) and the

117 targeted DNA sequence are perfectly complementary. Therefore, introducing mismatches
118 in the gRNA reduces the repression strength (29, 30). We generated a library of gRNAs
119 that permitted the expression of different quantities of AAC(6′)-Ib molecules, which were
120 quantified using a derivative of the pJHCMW1 plasmid that carries the native *aac(6')-Ib*
121 gene fused to the gene coding for the mNeonGreen fluorescent protein (Fig. 1A) (31). We
122 introduced this plasmid into *E. coli* strains harboring an IPTG-inducible dCas9-coding
123 gene and a constitutive gRNA-coding gene (Fig. 1B). The gRNA molecules in each strain
124 were designed to target different *aac(6')-Ib* regions (the promoter, the coding sequence,
125 or the linker, the coding or non-coding strand), and to have various degrees of
126 complementarity to the target sequence (Fig. 1A and Fig. S1). The effect of each gRNA
127 on the AAC(6′)-Ib expression level was assessed by spectrofluorometry on overnight LB
128 cultures supplemented with IPTG. The number of AAC(6′)-Ib molecules per cell obtained
129 using this methodology was corroborated by confocal microscopy (Fig. S2-3). The results
130 confirmed that dCas9 blocks the initiation and elongation of transcription and that the
131 length of complementarity to the target sequence is correlated with the strength of
132 repression. Targeting either strand of the *aac(6')-Ib* promoter provides strong
133 transcriptional repression (Fig. 1C). Guiding dCas9 binding to the coding strand of the
134 structural gene or the linker results in robust inhibition of gene expression. Conversely,
135 repression is not as pronounced when targeting the non-coding strand (Fig. 1D and E).
136 Reduction of the length of complementarity to the coding strand was associated with a
137 decrease in the degree of inhibition of gene expression (Fig. 1D and E). The results
138 described in this section indicate that the fluorescence-fusion system is adequate to
139 assess the number of AAC(6′)-Ib molecules per cell, and the CRISPRi fluorescence-

140 based system is an efficient tool to modulate the AAC(6′)-Ib copy number, spanning three
141 orders of magnitude.

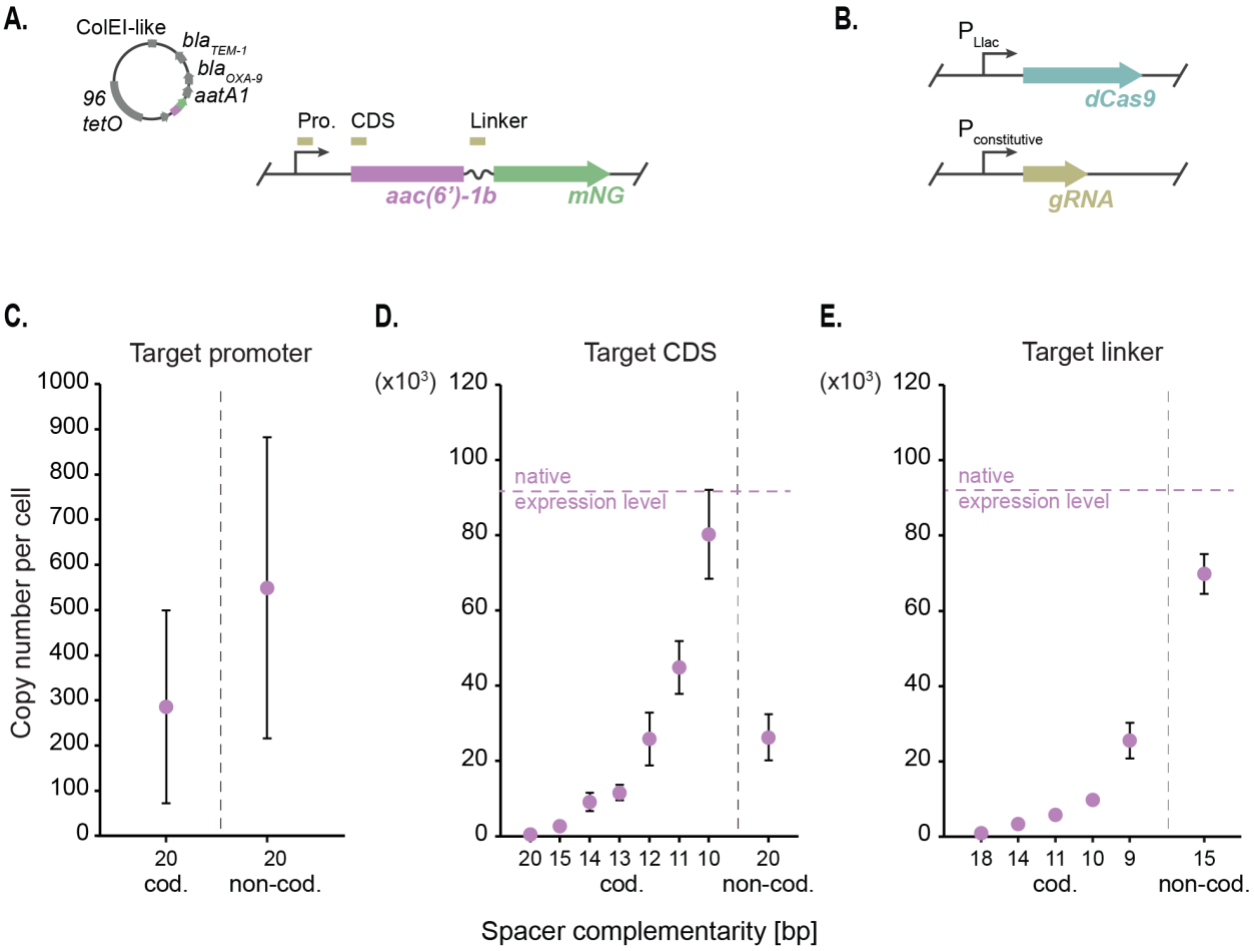

142

143 Figure 1 – Regulation of AAC(6′)-Ib copy number by CRISPRi. **A.** Schematic representation of the pJHCMW1 plasmid
144 and a zoomed view on the gene of interest, the aminoglycoside acetyltransferase AAC(6′)-Ib tagged with mNeonGreen
145 (mNG) under its native promoter. Boxes above the gene mark the regions targeted by the dCas9, which include the
146 promoter (Pro.), coding sequence (CDS), and linker. **B.** Schematic representation of the dCas9-coding gene under the
147 P_{Llac} promoter and the guide RNA (gRNA) with its constitutive promoter. **C.** Average AAC(6′)-Ib copy number per cell
148 obtained for strains harboring gRNAs with different complementarity to either the coding (cod.) or the non-coding strand
149 (non-cod.), varying lengths and targeting the promoter sequence, the CDS (**D.**) or the linker (**E.**) of the gene. Error bars
150 represent the standard deviation.

151

152 **At low copy numbers, the abundance of AAC(6′)-Ib and the minimum inhibitory**
153 **concentration of amikacin follow a linear relationship**

154 We carried out microtiter plate-based assays to evaluate how variations in the cellular
155 copy number of AAC(6′)-Ib impact amikacin-resistance levels. We determined the
156 amikacin concentration needed to reduce the culture OD_{600} value by 50%, defined as the
157 inhibitory concentration or IC_{50}. The native copy number of AAC(6′)-Ib in the strains used
158 is ∽92,000 molecules per cell, and the corresponding measured IC_{50} of amikacin was 135
159 μg/mL (Fig. 2A). Although such a high copy number is surprising, it is congruent with
160 expression of the gene from 20-30 copies of the plasmid from a strong promoter (15, 31).
161 Within a range spanning from none to about 10,000 AAC(6′)-Ib copies per cell, the IC_{50}
162 value increased as a function of the copy number, with an apparent relation of 1 μg/mL
163 resistance increase for every 170 AAC(6′)-Ib copies per cell (Fig. 2B). However, it was of
164 interest that this correlation ceased at ∽10,000 – 20,000 copies per cell when the
165 resistance level hit a plateau at IC_{50} of amikacin of 105 μg/mL. This value was constant,
166 up to ∽70,000 copies per cell, where the IC_{50} increased again up to 135 μg/mL (Fig. 2A).

167 As a point of reference, the "epidemiological cut-off value," which is defined as the
168 highest minimum inhibitory concentration (MIC) of the wild-type population, is reported to
169 be 8 μg/mL for enterobacteria (http://www.eucast.org) (32). In our conditions, a
170 concentration of 8 μg/mL is reached when the copy number of AAC(6′)-Ib per cell is ∽475.
171 While the conditions used to estimate this epidemiological cut-off value differ from those
172 used in this work, we expect that the minimum copy number of the enzyme needed to be

classified as resistant to amikacin should at least be in the same order of magnitude as our estimate.

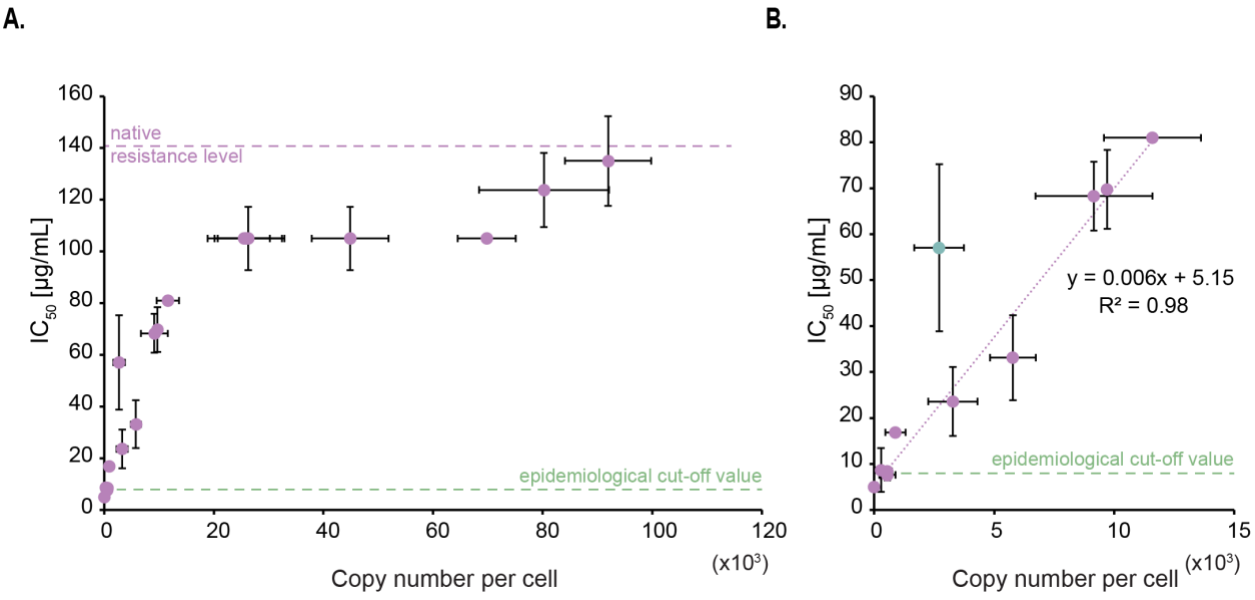

Figure 2 – Impact per AAC(6′)-Ib enzyme molecule on amikacin resistance level. **A.** Correlation between the inhibitory concentration at which 50% of the maximal culture density is observed (IC_{50}) and AAC(6′)-Ib copy number per cell. The native resistance level of the wild-type plasmid and the epidemiological cut-off value are also indicated (https://www.eucast.org). Error bars represent standard deviations. **B.** Lower copy numbers follow a linear relation with IC_{50} to amikacin. The linear trendline equation and its corresponding R-squared value are shown. The green dot represents an outlier that is excluded from the trendline.

AAC(6′)-Ib forms aggregates at higher concentrations

To gain insight into the correlation between protein copy number and resistance level described in the previous section, we further assessed the number of molecules per cell using confocal microscopy. The results of these assays showed that both techniques, spectrophotometry and microscopy, produced numbers per cell within the same order of

188 magnitude (Fig. S3). However, it was surprising to us that microscopy permitted us to
189 observe that the enzyme distributes homogeneously in the cytoplasm up to a specific
190 concentration, after which any increase tends to result in the formation of aggregates at
191 the cell poles (Fig. 3A). Low solubility and tendency to aggregate as inclusion bodies have
192 been observed before in a related variant (16).

193 The observed plateau in amikacin resistance may arise from AAC(6′)-Ib's inability to
194 exist in soluble and native form at copy numbers higher than 10,000 – 20,000. To test this
195 hypothesis, cells were cultured in broth supplemented with the chelating agent
196 ethylenediaminetetraacetic acid (EDTA), a compound known for disrupting ionic
197 interactions and favoring solubilization of protein aggregates. Fig. 3A shows that the
198 fluorescent protein was homogeneously distributed over the cytoplasm in cells cultured
199 in the presence of EDTA. In addition, Fig. 3B shows that the addition of EDTA did not
200 modify the number of molecules per cell, a clear indication that the sole effect of EDTA
201 was to dissolve the polar aggregates. Furthermore, the amikacin IC_{50} for cells cultured in
202 broth supplemented with EDTA increased as the AAC(6′)-Ib copy number increased (Fig.
203 3C). A comparison of the amikacin resistance levels in cells producing a number of
204 molecules consistent with the formation of aggregates but that were cultured in the
205 presence of the chelator showed a 1.5-fold increase in resistance. We conclude that
206 aggregation of AAC(6′)-Ib must inhibit enzymatic activity and is, at least in part,
207 responsible for the observed plateau effect.

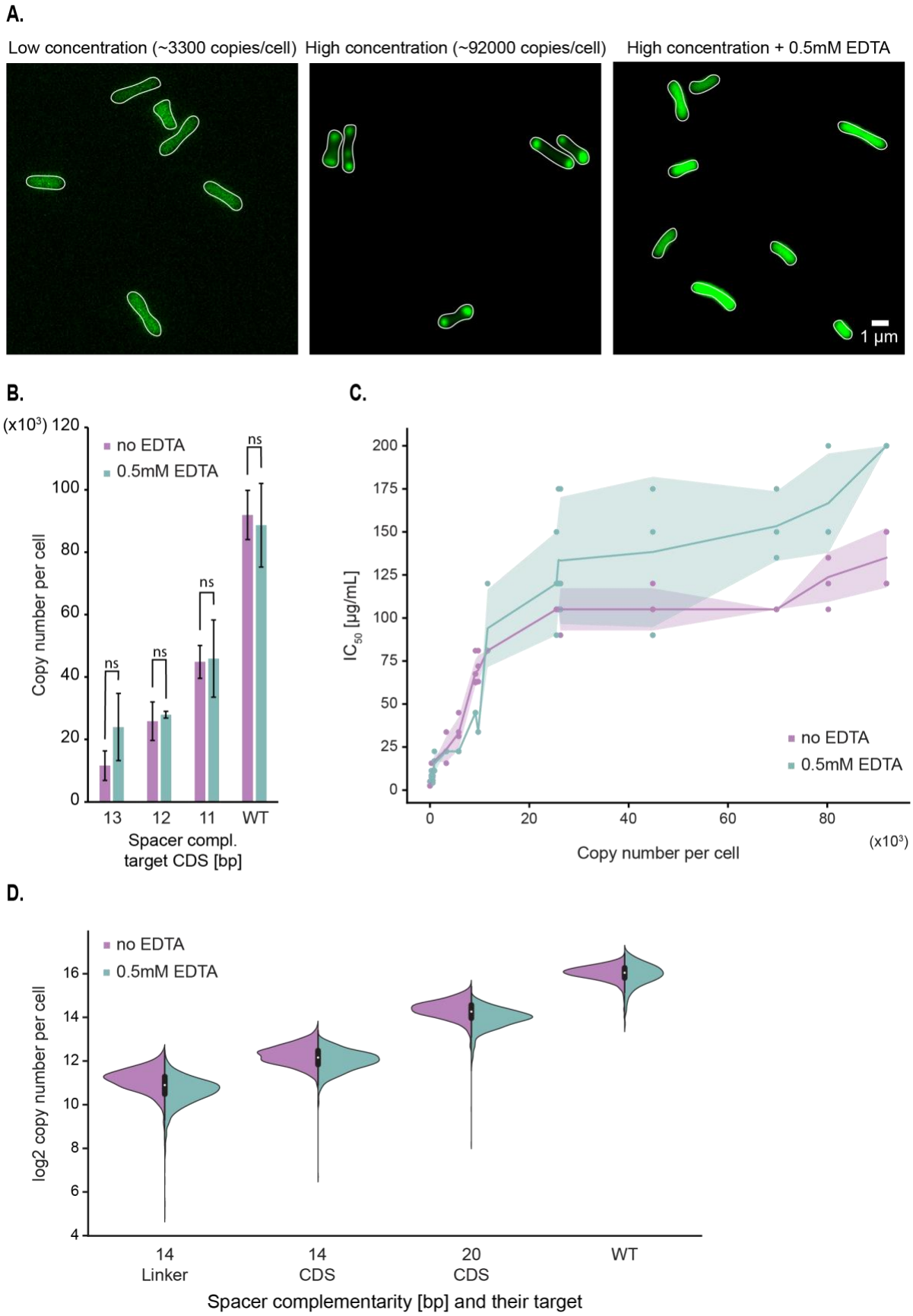
A.
Low concentration (~3300 copies/cell)
High concentration (~92000 copies/cell)
High concentration + 0.5mM EDTA
1 µm
B.
(x10³)
no EDTA
0.5mM EDTA
Copy number per cell
ns
13
12
11
WT
Spacer compl. target CDS [bp]
C.
IC50 [µg/mL]
no EDTA
0.5mM EDTA
Copy number per cell
(x10³)
D.
no EDTA
0.5mM EDTA
log2 copy number per cell
14 Linker
14 CDS
20 CDS
WT
Spacer complementarity [bp] and their target

208

209 Figure 3 – Formation of AAC(6′)-Ib aggregates at high protein concentrations partially inhibit enzyme activity against
210 amikacin. **A.** Representative images of strains carrying the pJHCMW1 plasmid derivative that encodes the *aac(6′)-Ib-*
211 *mNeonGreen* gene and the CRISPR-dCas9 system that targets the coding sequence (CDS) of this gene, with a strong
212 repression on the left and no repression in the middle image. The rightmost image displays the wild-type strain in
213 presence of 0.5 mM EDTA (ethylenediaminetetraacetic acid). **B.** Average copy number per cell of AAC(6′)-Ib in the
214 presence or absence of 0.5 mM EDTA, measured by spectrofluorometry. Each strain carries different lengths of gRNA
215 complementarity to the CDS of the *aac(6′)-Ib* gene. Error bars represent the standard deviation. A statistical analysis
216 compared the two conditions (ns, not significant for p=0.05). **C.** Scatterplot showing the relationship between AAC(6′)-
217 Ib copy number per cell and IC_{50} to amikacin. The shaded area represents the standard deviation in IC_{50}. **D.** Distribution
218 of AAC(6′)-Ib copy number, estimated with the confocal microscope, for strains encoding different guide RNAs in the
219 presence or absence of 0.5 mM EDTA. Complementarity of the gRNA to the coding strand of the *aac(6′)-Ib* gene is
220 indicated for each strain.

221 **Diversity of AAC(6′)-Ib expression profile per cell within a population**

222 While estimations of protein expression per cell are reproducible, measurements
223 made with the fluorometer do not provide any information regarding the variability of gene
224 expression within a population. The confocal microscope, however, allows an estimation
225 of AAC(6′)-Ib copy number at the single-cell level, revealing potential cell-to-cell variation.
226 This is particularly important in the case of strains where the expression of AAC(6′)-Ib is
227 regulated by CRISPRi. If there was cell-to-cell variability in the levels of dCas9, the
228 individual cell's AAC(6′)-Ib copy numbers could be significantly different, which would
229 cloud the interpretation of our results. However, the results showed that AAC(6′)-Ib
230 expression is normally distributed in the cell population of individual strains (Fig. 3D and
231 Table S4). Also, cell-to-cell fluctuations in the protein concentration were similar to
232 changes at native expression levels. These results indicated that our CRISPRi system
233 has no impact on the intrinsic variations of AAC(6′)-Ib expression. Importantly, this

234 experiment also confirmed that the presence of EDTA in the cell's environment does not
235 modify the protein's copy number or cell-to-cell variability.

236 **AAC(6′)-Ib diffuses freely in the cell**

237 To further understand the dynamics of AAC(6′)-Ib within the cytosol, we characterized
238 its diffusion properties using single-particle tracking via Photoactivated Localization
239 Microscopy (sptPALM) (33). We used a fusion of AAC(6′)-Ib with the photoconvertible
240 fluorescent protein mMaple (34) and captured images at 20-ms rates. To study the
241 dynamics of single molecules, we exposed cells to continuous 405 nm light at low
242 intensity, conditions that result in the activation of a single molecule of mMaple per cell,
243 on average. The resulting images permitted us to track a molecule's position and follow
244 its trajectory (Fig. 4A). Tracked molecules of AAC(6′)-Ib covered all the cytosol, with no
245 location preference or obvious binding to any cellular structure. The average apparent
246 diffusion coefficient of AAC(6′)-Ib diffusing in the cell is the same as that of mMaple alone
247 (Fig. 4B). In conclusion, the results described in this section indicate that in the absence
248 of aggregation, AAC(6′)-Ib molecules diffuse freely across the cytosol.

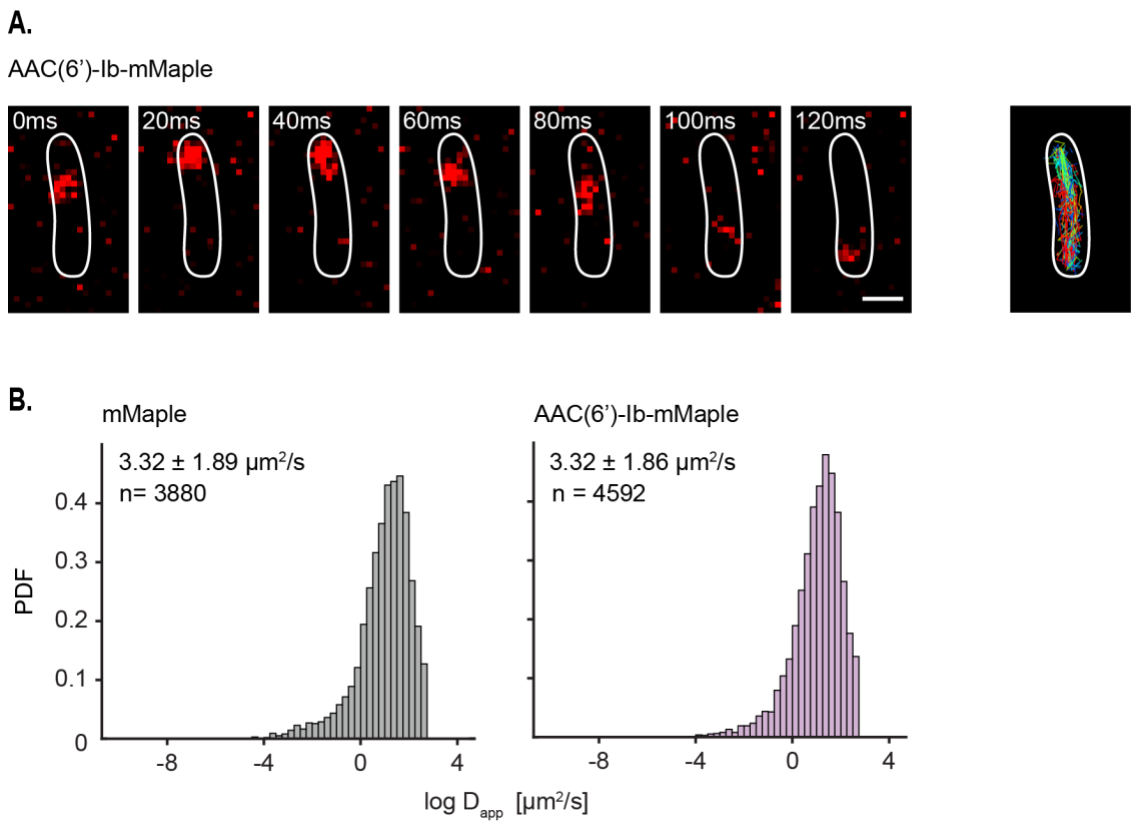

Figure 4 – AAC(6′)-Ib is highly dynamic in the cells. **A.** Representative images of AAC(6′)-Ib-mMaple foci every 20 ms. Tracks are represented on the rightmost image. Scale bar: 1μm. **B.** Distribution of the logarithm of the apparent diffusion coefficient (D_{app}) for mMaple (left) and AAC(6′)-Ib-mMaple (right). The y axis represents the probability density function (PDF). The apparent diffusion coefficient of the diffusing fraction, taken from the exponential of the mu and sigma obtained from the Gaussian distribution, and the total amount of tracks analyzed are indicated.

255 ## Discussion

256 The rapid dissemination of aminoglycoside modifying enzymes has severely reduced
257 the effectiveness of aminoglycosides. The acetyltransferase AAC(6′)-Ib is among the
258 most clinically relevant due to its ability to catalyze the inactivation of numerous
259 aminoglycosides used to treat severe infections. The substrates of AAC(6′)-Ib include
260 natural as well as semisynthetic aminoglycosides such as amikacin (7, 11, 13). The
261 *aac(6′)-Ib* gene, as well as the AAC(6′)-Ib protein, have been the subject of intense
262 genetic, structural, and biochemical studies (7, 13, 16, 17, 35, 36). However, despite
263 these advances, numerous unanswered questions remain; clarifying these is critical for
264 the rational design of novel therapies.

265 To reduce the knowledge gap, we studied the dynamics of the AAC(6′)-Ib protein
266 inside the cytosol to assess how its copy number variation impacts amikacin resistance.
267 To do so, we devised methodologies to quantify and control AAC(6′)-Ib copy number. A
268 fusion AAC(6′)-Ib-mNeonGreen enabled us to quantify the number of protein molecules
269 per cell using fluorometry and confocal microscopy. Then, we used a CRISPRi system to
270 produce strains that expressed a wide range of molecules per cell. These tools were used
271 to compare amikacin resistance levels in strains harboring different numbers of enzyme
272 molecules. We observed a close correlation between resistance levels and the number
273 of protein molecules at low concentrations. These results agree with previous reports that
274 the copy number of different resistance genes is amplified in mutants displaying increased
275 resistance (21-27). However, previous studies were limited to correlating the number of
276 gene copies, increased by amplification mechanisms or modification of plasmid copy

277 numbers and resistance levels. Absent in these reports are correlations of actual
278 expressed resistance enzyme molecules and resistance levels. This work now accurately
279 measured amikacin resistance as a function of AAC(6′)-Ib copy number.

280 Our results indicate that resistance levels reach a plateau at a certain level of AAC(6′)-
281 Ib concentration. The single-cell results obtained by microscopy showed that the AAC(6′)-
282 Ib molecules tend to aggregate and localize at the poles in structures resembling inclusion
283 bodies at higher concentrations. This observation, taken together with the well-known fact
284 that the protein has limited water solubility (16), explains, at least in part, the lack of
285 correlation between the AAC(6′)-Ib copy number and resistance levels at higher protein
286 concentrations. Physical exclusion of AAC(6′)-Ib, due to the formation of inclusion bodies,
287 can limit its accessibility to the antibiotic molecules. Adding EDTA to the growth medium
288 quantified the contribution of aggregate formation to the observed plateau in resistance
289 levels. The chelator's presence interfered with the formation of AAC(6′)-Ib aggregates and
290 was correlated with an increase in the amikacin IC_{50}. Not only do these results associate
291 aggregation with increased resistance, but they also suggest that the process is
292 structurally dynamic and reversible. This behavior will be essential to consider when
293 developing strategies to inhibit resistance. For example, antisense inhibition of AAC(6′)-
294 Ib expression, a methodology that attempts phenotypic conversion to susceptibility by
295 turning off gene expression, will need to be very efficient to reduce the number of proteins
296 produced well below the aggregation threshold.

297 Another potential contributor to the plateau observed is enzyme kinetics. The classic
298 expectation that the enzymatic reaction velocity increases linearly with enzyme
299 concentration is valid only when the substrate is present at much higher concentrations

300 than the enzyme. For amikacin resistance, substrates inside the cytosol may not saturate
301 the enzyme. The intracellular concentrations of acetyl-CoA, the acyl donor, have been
302 reported to be in the 20-600 μM range (37), which are comparable to those estimated for
303 AAC(6′)-Ib in strains producing high copy numbers (40-150 μM). Availability of acetyl-CoA
304 may limit the enzyme activity rate. Also, amikacin concentrations inside the cytosol are
305 likely lower than those in the growth medium (note that 125 μg/ml equals 160 μM). Hence,
306 the substrates/enzyme concentration ratios may also influence the resistance levels in
307 growing cells. While the enzyme solubility issue seems to affect our results, future
308 experiments must be planned to help understand the enzyme kinetics in the cytosol.
309 Adding to these complications, one must consider that different bacteria will have different
310 permeabilities to the antibiotic and could possess efflux pumps.

311 Our previous studies showed that unlike other resistance enzymes like β-lactamases
312 that are periplasmic (38), AAC(6′)-Ib is uniformly distributed within the cytoplasm (14, 39).
313 However, those experiments required overexpression of the enzyme, which could have
314 modified the subcellular location at physiological levels. The methodology used in this
315 work corroborated our early results and further illustrated the dynamics of AAC(6′)-Ib
316 inside the cytosol. The protein can traverse the length of the cell in ~100 ms.

317 In conclusion, this work makes inroads in understanding the individual contribution of
318 AAC(6′)-Ib molecules to resistance to aminoglycosides and clarifies its dynamics inside
319 the cell. Importantly, it opens the doors to understanding the role of solubility and
320 expression levels in the resistance phenotype. We expect that the system we devised will
321 help us better understand antibiotic resistance from cellular and molecular biology
322 perspectives.

323

324

325

326

327 ## Materials and methods

328 ### Strains and growth conditions

329 All strains used are derivatives of AB1157 (Table S1). Cells were routinely grown in
330 LB or M9 minimal media. M9 was supplemented with glycerol (final concentration 0.2%);
331 100 µg/ml of amino acids threonine, leucine, proline, histidine, and arginine; and thiamine
332 (0.5 µg/ml). When required, antibiotics were added at the following concentrations:
333 ampicillin (100 µg/ml), kanamycin (50 µg/ml), and chloramphenicol (25 µg/ml). The TB25
334 strain was constructed by chromosomal integration of the P_{lacq}-*lacI* $P_{Llac\text{-}s}$-*dCas9* gene
335 from the pTB35 plasmid at the lambda *attB* site (40). Each gRNA was inserted into the
336 pTB40-1 plasmid through site-directed mutagenesis that was carried out by uracil-specific
337 excision reagent (USER) cloning (Table S2) (41). The different gRNAs were further
338 integrated by lambda red in the *argE* gene. OD030 was constructed using lambda red
339 recombination with the pROD93 plasmid carrying the *mMaple* gene, which was inserted
340 into the *galK* gene. The mNeonGreen gene was integrated into the pTT4 plasmid (15) to
341 generate pTT4-mNG-wL, and the construction was subsequently sequenced by whole
342 plasmid sequencing service of plasmidsaurus (www.plasmidsaurus.com). The pFH3
343 plasmid is a pTT4-mNG-wL derivative where the *mNeonGreen* gene was replaced by
344 *mMaple3* by *Nco*I digestion and ligation. All primers used for these constructions are
345 described in Table S3.

346 **Protein expression and purification**

347 Fluorescent proteins were produced using pROD93 expression vector in BL21(DE3)
348 strains. Cells were grown at 37°C until they reached an OD_{600} ~ 0.6. Protein expression
349 was then induced by adding 0.2% of L-arabinose and incubating the culture at 30°C. After
350 4 hours of induction, bacteria were centrifuged and the pellet was resuspended in
351 Resuspension Buffer (25 mM Tris HCl pH 7.5, 250 mM NaCl) supplemented with one
352 tablet of cOmplete protease inhibitor (Roche, Cat # 04693159001). Cells were then lyzed
353 using a high-pressure Emulsiflex C5 homogenizer (Avestin), and the lysate was cleared
354 by ultra-centrifugation (35 000 rpm, 1 hour, 4°C). The lysate was added to the Ni-IDA resin
355 (Takara, Cat # 635660) equilibrated with Binding Buffer (50 mM NaPi, 20 mM Imidazole,
356 300 mM NaCl, 10% glycerol, pH 8) and incubated for at least an hour at 4°C. The resin
357 was transferred to a disposable column and washed out at least 5 times with Binding
358 Buffer and twice with Binding Buffer that has a higher concentration of imidazole (40 mM).
359 Protein was eluted in Elution Buffer (50 mM NaPi, 200 mM Imidazole, 300 mM NaCl, 10%
360 glycerol, pH 8). The protein was then dialyzed in Slide-A-Lyzer MINI Dialysis Devices
361 immersed in the Storage Buffer (25 mM Tris HCl pH8, 300 mM NaCl, 10% glycerol) and
362 finally stored, protected from light, at -20°C.

363 **Fluorometer calibration assay**

364 For mNG fluorescence calibration, the purified protein stock was first diluted in M9
365 minimal media to a concentration of 2.5 10^{-2} mg/mL and then diluted 1:2 for a total of 7
366 dilutions. 200µL of each concentration was distributed in a black microplate (Fisher, Cat
367 # 7200590), and the total intensity was measured with a Cary Eclipse Fluorescence

368 Spectrophotometer (Agilent Technologies) at 500 nm for excitation and 530 nm for
369 emission. The slits were set to 10 and 20 nm for excitation and emission, respectively.
370 After correcting for the background fluorescence of M9 minimal media, we could estimate
371 the average fluorescence intensity per mNG protein.

372 **Fluorometer-based copy number quantification**

373 The strains expressing the dCas9 with the different gRNAs and carrying the pTT4-
374 mNG-wL plasmid were first grown overnight in LB media in the presence of ampicillin and
375 1 mM IPTG at 37°C. The OD_{600} of the culture was measured, and 1 mL was washed in
376 M9 minimal media, from which 200 µL were distributed in a clear 96-well plate as
377 triplicates. Using the same parameters as in the fluoromoter calibration assay, the total
378 fluorescence was measured using the Cary Eclipse fluorometer. AAC(6′)-Ib copy number
379 could thus be estimated by dividing the measured intensity by the OD_{600}, correcting for
380 the fluorescence of the cells without the fluorescent plasmid and dividing by the average
381 fluorescence intensity per mNG molecule (4.92×10^{-12}, Fig. S2). This value was then
382 divided by the estimated bacterial count (5.22×10^{8} CFU/OD_{600}/mL) to calculate the copy
383 number per cell.

384 **Copy number estimation using the confocal microscope**

385 Single-molecule mNG intensity was quantified using the YHZ23 strain that carries a
386 mNG-tagged Nup59, a well-characterized 16-mer component of the nucleopore complex
387 (NPC) in budding yeast. This strain was imaged using a custom-built spinning disk
388 confocal microscope (Leica DMi8 inverted microscope with Quorum Diskovery platform,
389 50 µm pinhole spinning disk and two iXon Ultra 512x512 EMCCD cameras). A single

390 colony was grown in synthetic complete (SC) media, with shaking, for 5 hours at 30°C.
391 This culture was diluted 100 times and cultured overnight in the same conditions before
392 being diluted again to an OD_{600} of 0.15 and incubated until it reached 0.3. 1mL of this
393 culture was spun down and concentrated twice in fresh SC media before being spread
394 on a 1% agarose pad. Imaging was performed by taking 10 z-stacks of 0.59μm step size
395 with 488 nm laser at 25% intensity and with a 200ms exposure time. Single spots were
396 identified manually throughout the z-stacks and were subsequently fitted to 2D Gaussian
397 with the GaussFit on Spot plugin in ImageJ. Using Matlab, the intensity values were fitted
398 to a Gaussian Mixture Model, resulting in two distinct components (Nup59 from single
399 and double NPCs). The mean of the first component, *i.e.,* in the single NPC, is the
400 intensity of 16 mNG molecules (mean intensity = 11374.4 and thus intensity of a single
401 mNG = 710.9).

402 As for the fluorometer-based quantification, bacterial cultures were incubated
403 overnight in LB media in the presence of ampicillin and 1 mM IPTG at 37°C. Imaging was
404 performed by taking 7 z-stacks of 0.59μm step size with 488 nm laser at 25% intensity
405 and with a 200ms exposure time. Stacked images were projected for analysis by
406 summing all pixel values at each position. Images were then segmented with Cellpose,
407 and the total intensity per cell was quantified using custom Fiji and Python scripts.

408 **IC_{50} determination**

409 Cells were first cultured overnight in LB medium in the presence of ampicillin and 1
410 mM IPTG. They were then diluted 1:10000 in fresh LB, and 5μL was added into each well
411 of a 96-well microtitre plate (Sarstedt, Cat # 82.1581.001) carrying 100μL LB of a series

412 of 2-fold dilutions of amikacin as well as 1mM IPTG. When desired, the LB media was
413 also supplemented with 0.5 mM EDTA. The plate was then incubated for 20 hours at
414 37°C. IC_{50} was defined as the lowest antibiotic concentration at which half of the bacterial
415 growth is inhibited.

416 **Single molecule experiments and analysis**

417 Overnight bacterial cultures were diluted in M9 minimal media supplemented with 1
418 mM IPTG and cultured until they reached early logarithmic phase (OD_{600} of 0.1-0.2). Cells
419 were then visualized with an inverted Olympus IX83 microscope at room temperature. A
420 Hamamatsu Orca-Flash 4.0 sCMOS camera was used for image capturing, and Z-stacks
421 were done using a NanoScanZ piezo by Prior Scientific. Excitation was performed with
422 an iChrome Multi-Laser Engine from Toptica Photonics, combined with a
423 405/488/561/640nm filter set (Chroma). We used a Single-line cellTIRF illuminator
424 (Olympus) for the experiments, and the Olympus CellSens 2.1 imaging software was
425 used to control the microscope and the lasers. All data analyses were performed using
426 custom MATLAB scripts (Mathworks), except for single molecule tracking that was done
427 using Trackmate (42, 43).

428

429 ## Acknowledgments

430 We thank Jia Yin Xiao for sharing microscope single-molecule calibration data. The Reyes
431 lab was funded by the Natural Sciences and Engineering Research Council of Canada
432 (NSERC RGPIN-2019-05701), the Canadian Institutes for Health Research (CIHR PJT-

433 162247), the Canada Foundation for Innovation (CFI# 228994), and the Canada
434 Research Chairs program. The Tolmasky lab was funded by Public Health Service Grant
435 2R15AI047115-06 (National Institute of Allergy and Infectious Diseases, NIH) and the
436 Ramirez lab was funded by Public Health Service Grant SC3GM125556 (National
437 Institute of General Medical Sciences, NIH). Fong Hue was supported by grant MHRT
438 2T37MD001368 from the National Institute on Minority Health and Health Disparities,
439 NIH. Some of the experiments used equipment from the Integrated Quantitative
440 Bioscience Initiative (IQBI), funded by CFI 9.

441 *Author contributions:* O.D.D.: Conceptualization, Formal analysis, Investigation, and
442 Writing. F.H.: Formal analysis and Investigation, T.Y: Formal analysis and Investigation.
443 L.W.: Formal analysis and Investigation. M.L.: Formal analysis and Investigation. L.R.:
444 Formal analysis and Investigation. M.S.R.: Formal analysis and Investigation. W.R:
445 Conceptualization and Writing. M.E.T.: Conceptualization, Supervision, Funding
446 acquisition and Writing. R.R.-L.: Conceptualization, Supervision, Funding acquisition and
447 Writing.

Supplementary data

Figure S1 – dCas9 targets (Promoter, CDS and Linker on both the coding (cod.) and non-coding (non-cod.) strands) in the *aac(6')-Ib* gene on the pJHCMW1-derivative plasmid. The complementary sequence to the gRNA (green bar) is highlighted in green and the blue arrow represents the positions at which the mismatches in the sequence of the gRNA were introduced. The *aac(6')-Ib* START codon is indicated in red and the number of base pairs not included in this representation are indicated in parenthesis.

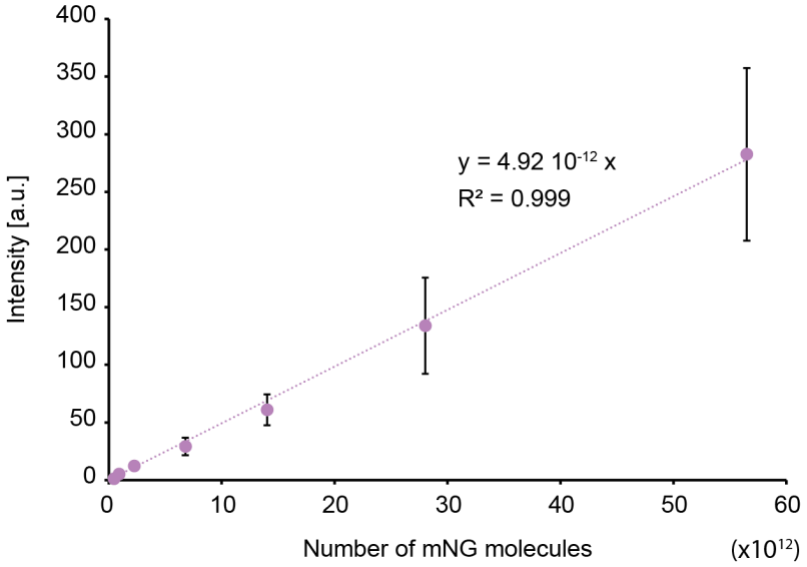

Figure S2 – Calibration curve between mNeonGreen intensity measured by spectrofluorometry (in arbitrary units, a.u.) and the number of mNeonGreen molecules. The equation of the linear trendline, as well as the correlation coefficient (R^2), are indicated on the plot.

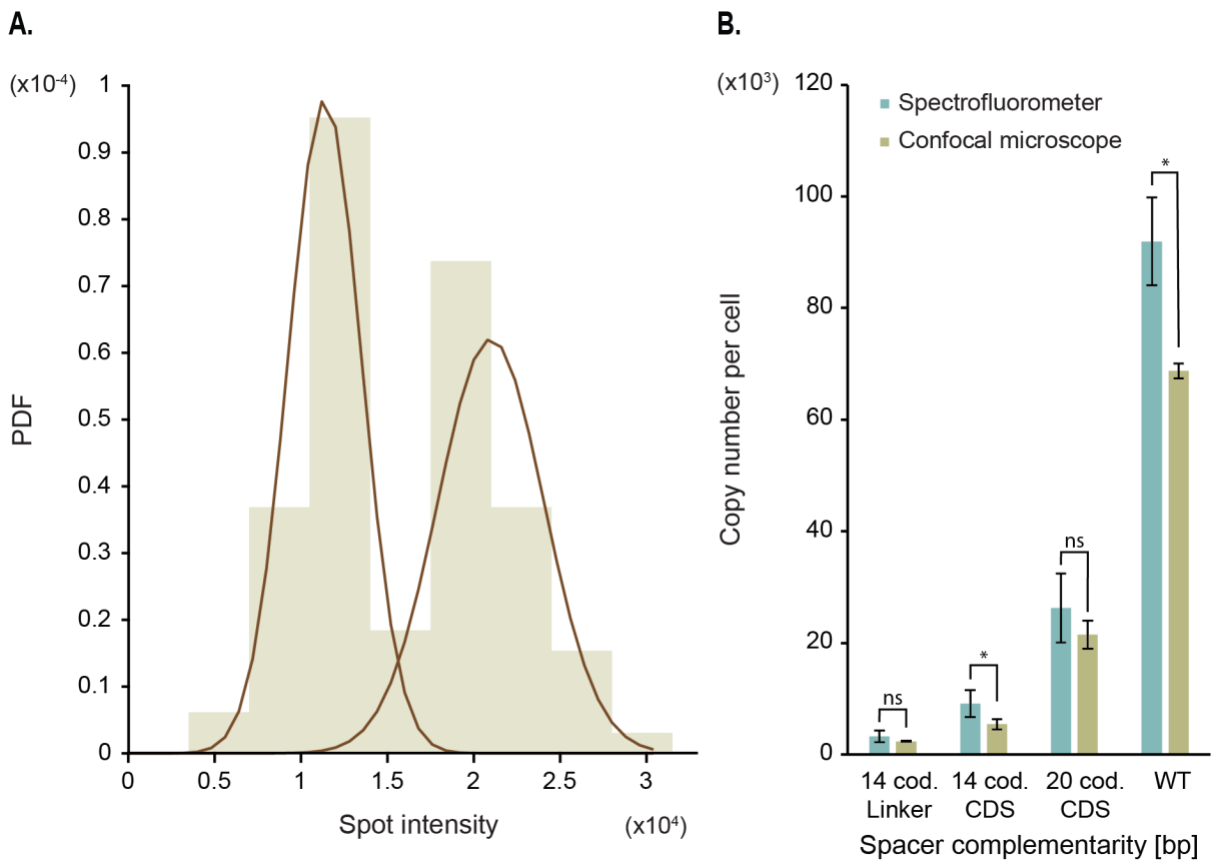

Figure S3 – Confirmation of AAC(6′)-Ib copy number by confocal microscopy. **A.** mNeonGreen intensity per molecule, estimated by imaging Nup59-mNeonGreen. The brown lines represent the Gaussian Mixture Model fitted to each population. The one on the left represents the 16-mer Nup59 (mean intensity = 11374.4), and the second peak carries 32 Nup59 (mean intensity = 20988.6). This gives an average intensity of 710.9 per mNeonGreen molecule. In total, 93 spots are represented in this plot. **B.** AAC(6′)-Ib copy number estimated with the spectrofluorometer (blue bars) and with the confocal microscope (green bars) for four strains, each carrying a different guide RNA. The length of the gRNA that is complementary to the coding (cod.) strand, as well as the targeted region of the *aac(6')-Ib* gene, are indicated. Error bars represent the standard deviation and comparative statistical analysis was performed to compare the two methods (ns, not significant, and *, significant for p=0.05).

474 Table S1 - Strains used for this study.

Strain	**Relevant genotype**	**Source**
AB1157	*thr-1*, *araC14*, l*euB6*(Am), DE(*gpt-proA*)62, *lacY1*, *tsx33*, qsr'-0, *glnV44*(AS), *galK2*(Oc), LAM$^-$, Rac-0, *hisG4*(Oc), *rfbC1*, *mgl-51*, *rpoS396*(Am), *rpsL31*(str^R), *kdgK51*, *xylA5*, mtl-1, *argE3*(Oc), *thi-1*	(44)
BL21(DE3)	*fhuA2* [lon] *ompT gal* [*dcm*] Δ*hsdS*	(45)
TB25	AB1157 derivative, P_{lacq}-*lacI* $P_{Llac\text{-}s}$-*dCas9 cat::ΔattB*	This work
FHcas1nc	TB25 derivative, *gRNA-Prom (20bp cod.)::argE*	This work
FHcas1	TB25 derivative, *gRNA-Prom (20bp non-cod.)::argE*	This work
FHcas2nc	TB25 derivative, *gRNA-CDS (20bp cod.)::argE*	This work
LW3	TB25 derivative, *gRNA-CDS (15bp cod.)::argE*	This work
TY1	TB25 derivative, *gRNA-CDS (14bp cod.)::argE*	This work
LW2	TB25 derivative, *gRNA-CDS (13bp cod.)::argE*	This work
LW1	TB25 derivative, *gRNA-CDS (12bp cod.)::argE*	This work

TY2	TB25 derivative, *gRNA-CDS (11bp cod.)::argE*	This work
TY3	TB25 derivative, *gRNA-CDS (10bp cod.)::argE*	This work
FHcas2	TB25 derivative, *gRNA-CDS (20bp non-cod.)::argE*	This work
FHcas3nc	TB25 derivative, *gRNA-Linker (18bp cod.)::argE*	This work
TY4	TB25 derivative, *gRNA-Linker (14bp cod.)::argE*	This work
TY5	TB25 derivative, *gRNA-Linker (11bp cod.)::argE*	This work
TY6	TB25 derivative, *gRNA-Linker (10bp cod.)::argE*	This work
LW4	TB25 derivative, *gRNA-Linker (9bp cod.)::argE*	This work
FHcas3	TB25 derivative, *gRNA-Linker (15bp non-cod.)::argE*	This work
OD030	P_{Lac}*-mMaple kan::ΔgalK*	This work
YHZ23	*MATa his3Δ1 leu2Δ0 met15Δ0 LYS2 ura3Δ0 nup59-mNeonGreen-Nat*	This work

475

476

477 Table S2 – Plasmids used in this study.

Plasmid	**Description**	**Source**
pTT4	pJHCMW1 derivative containing 96 copies of *tetO* inserted into the *tnpA* gene.	(15)
pTT4-mNG-wL	pTT4 derivative carrying an *aac(6')-Ib-mNeonGreen* fusion.	This work
pFH3	pTT4 derivative carrying an *aac(6')-Ib-mMaple* fusion.	This work
pROD93	Plasmid containing the *mMaple* gene under a P_{Llac} promoter, with an R6K gamma origin and kanamycin resistance.	(33)
pTB35	Plasmid carrying the *dCas9* gene under P_{Llac} promoter with constitutive lac. Used for *attP* integration with chloramphenicol resistance.	(46)
pTB40-1	Plasmid expressing dnaX-targetting gRNA. R6K gamma *ori*.	This work

478

479 **Table S3 –** Primers used in this work. The guide RNA sequences are highlighted in green, while the mutated base pairs
480 are shown in blue. cod., coding, non-cod., non-coding, compl., complementary, CDS, coding sequence.

Primer	Sequence 5'-3'	Description
TB04	ACTAGTAUTATACCTAGGACTGAG	Fixed primer for gRNA mutagenesis on the pTB40-1 plasmid
FHcas1	ATACTAGUTGCTTCAATAATATTGAAAAGTTTTAGAGCTAGAAATAGCAAG	Primer for gRNA mutagenesis of the pTB40-1 plasmid. 20bp compl. to non-cod. strand of promoter.
FHcas1nc	ATACTAGUCAGGGTTATTGTCTCATGAGGTTTTAGAGCTAGAAATAGCAAG	Primer for gRNA mutagenesis of the pTB40-1 plasmid. 20bp compl. to cod. strand of promoter.
FHcas2	ATACTAGUCAACATTTCCAAACAAAGTTGTTTTAGAGCTAGAAATAGCAAG	Primer for gRNA mutagenesis of the pTB40-1 plasmid. 20bp compl. to non-cod. strand of CDS.
FHcas2nc	ATACTAGUTTGTGATGCCTAACTTTGTTGTTTTAGAGCTAGAAATAGCAAG	Primer for gRNA mutagenesis of the pTB40-1 plasmid. 20bp compl. to cod. strand of CDS.
FHcas3	ATACTAGUGCCATGGCTGGCTCCGCTGCGTTTTAGAGCTAGAAATAGCAAG	Primer for gRNA mutagenesis of the pTB40-1 plasmid. 15bp compl. to non-cod. strand of linker.
FHcas3nc	ATACTAGUGACTGCGCCAGAACCAGCAGGTTTTAGAGCTAGAAATAGCAAG	Primer for gRNA mutagenesis of the pTB40-1 plasmid. 18bp compl. to cod. strand of linker.
14bpFHcas2nc	ATACTAGUAACACTTGCCTAACTTTGTTGTTTTAGAGCTAGAAATAGCAAG	Primer for gRNA mutagenesis of the pTB40-1 plasmid. 14bp compl. to cod. strand of CDS.

11bpFHcas2nc	ATACTAGUAACACTACGCTAACTTTGTTGTTTTAGAGCTAGAAATAGCAAG	Primer for gRNA mutagenesis of the pTB40-1 plasmid. 11bp compl. to cod. strand of CDS.
10bpFHcas2nc	ATACTAGUAACACTACGGTAACTTTGTTGTTTTAGAGCTAGAAATAGCAAG	Primer for gRNA mutagenesis of the pTB40-1 plasmid. 10bp compl. to cod. strand of CDS.
14bpFHcas3nc	ATACTAGUCTGACGGCCAGAACCAGCAGGTTTTAGAGCTAGAAATAGCAAG	Primer for gRNA mutagenesis of the pTB40-1 plasmid. 14bp compl. to cod. strand of linker.
11bpFHcas3nc	ATACTAGUCTGACGCGGAGAACCAGCAGGTTTTAGAGCTAGAAATAGCAAG	Primer for gRNA mutagenesis of the pTB40-1 plasmid. 11bp compl. to cod. strand of linker.
10bpFHcas3nc	ATACTAGUCTGACGCGGTGAACCAGCAGGTTTTAGAGCTAGAAATAGCAAG	Primer for gRNA mutagenesis of the pTB40-1 plasmid. 10bp compl. to cod. strand of linker.
12bpFHcas2nc	ATACTAGUAACACTACCCTAACTTTGTTGTTTTAGAGCTAGAAATAGCAAG	Primer for gRNA mutagenesis of the pTB40-1 plasmid. 12bp compl. to cod. strand of CDS.
13bpFHcas2nc	ATACTAGUAACACTAGCCTAACTTTGTTGTTTTAGAGCTAGAAATAGCAAG	Primer for gRNA mutagenesis of the pTB40-1 plasmid. 13bp compl. to cod. strand of CDS.
15bpFHcas2nc	ATACTAGUAACACATGCCTAACTTTGTTGTTTTAGAGCTAGAAATAGCAAG	Primer for gRNA mutagenesis of the pTB40-1 plasmid. 15bp compl. to cod. strand of CDS.
9bpFHcas3nc	ATACTAGUCTGACGCGGTCAACCAGCAGGTTTTAGAGCTAGAAATAGCAAG	Primer for gRNA mutagenesis of the pTB40-1 plasmid. 9bp compl. to cod. strand of linker.
TB200	ATAAATACTGCATGAATATTGATACTATCATGACCAGAGGTGTGTCAACATTTCGCTAAGGATGATTTCTGG	Primer to insert each gRNA into *argE* gene by lambda red.

TB201	CGGATGCGGCGCGAGCGCCTTATCCGGCCTACGTTTTAATGCCAGCATATCCTCCTTAGTTCCTATTCC	Primer to insert each gRNA into *argE* gene by lambda red.
mMapleNcoI_F	TTTCCATGGCTGGCTCCGCTGCTGGTTC	Primer to clone *mMaple* into pTT4 by *Nco*I digestion.
mMapleNcoI_R	TTTCCATGGTTACTTGTACAGCTCGTCCATGC	Primer to clone *mMaple* into pTT4 by *Nco*I digestion.
galK_insF	GTTTGCGCGCAGTCAGCGATATCCATTTTCGCGAATCCGGAGTGTAAGAACGCCCAATACGCAAACCG	Primer to insert *pLac-mMaple* into *galK* gene by lambda red.
galK_insR	CGGCTGACCATCGGGTGCCAGTGCGGGAGTTTCGTTCAGCACTGTCCTGCCTTATGAATATCCTCCTTAG	Primer to insert *pLac-mMaple* into *galK* gene by lambda red.

481

482

483 **Table S4 –** Number of repeats and total cell count for Figure 3.D

Strain	Treatment	Number of repeats	Total number of cells	Average copy number ± Standard deviation
TY4	/	3	2402.99 ± 852.69	1212
	EDTA	3	1681.9 ± 689.61	1492
TY1	/	3	5193.5 ± 1673.95	1673
	EDTA	3	4299.94 ± 1375.28	1365
FHcas2	/	3	21798.56 ± 6187.83	1633
	EDTA	3	16461.43 ± 4888.06	639
TB25	/	3	68815.57 ± 15122.08	1900
	EDTA	3	67141.91 ± 21968.79	873

484

485 ## References

486 1. Boucher HW. 2020. Bad bugs, no drugs 2002-2020: progress, challenges, and call to action.
487 Trans Am Clin Climatol Assoc 131:65-71.

488 2. Murray C, Ikuta K, Sharara F, Swetschinski L, Aguilar G, Gray A, Han C, Bisignano C, Rao P,
489 Wool E, Johnson S, Browne A, Chipeta M, Fell F, Hcket S, al e. 2022. Global burden of
490 bacterial antimicrobial resistance in 2019: a systematic analysis. Lancet 399:629-655.

491 3. Butler MS, Gigante V, Sati H, Paulin S, Al-Sulaiman L, Rex JH, Fernandes P, Arias CA, Paul
492 M, Thwaites GE, Czaplewski L, Alm RA, Lienhardt C, Spigelman M, Silver LL, Ohmagari N,
493 Kozlov R, Harbarth S, Beyer P. 2022. Analysis of the clinical pipeline of treatments for drug-
494 resistant bacterial infections: despite progress, more action Is needed. Antimicrob Agents
495 Chemother 66:e0199121.

496 4. Tolmasky ME. 2017. Strategies to prolong the useful life of existing antibiotics and help
497 overcoming the antibiotic resistance crisis, p 1-27. *In* Atta-ur-Rhaman (ed), Frontiers in
498 Clinical Drug Research-Anti Infectives, vol 1. Bentham Books, Sharjah, UAE.

499 5. Kaul M, Barbieri CM, Pilch DS. 2004. Fluorescence-based approach for detecting and
500 characterizing antibiotic-induced conformational changes in ribosomal RNA: comparing
501 aminoglycoside binding to prokaryotic and eukaryotic ribosomal RNA sequences. J Am
502 Chem Soc 126:3447-53.

503 6. Krause KM, Serio AW, Kane TR, Connolly LE. 2016. Aminoglycosides: an overview. Cold
504 Spring Harb Perspect Med 6:a027029.

505 7. Ramirez MS, Tolmasky ME. 2010. Aminoglycoside modifying enzymes. Drug Resist Updat
506 13:151-71.

507 8. Wohlgemuth I, Garofalo R, Samatova E, Gunenc AN, Lenz C, Urlaub H, Rodnina MV. 2021.
508 Translation error clusters induced by aminoglycoside antibiotics. Nat Commun 12:1830.

509 9. Bottger EC, Crich D. 2020. Aminoglycosides: time for the resurrection of a neglected class
510 of antibacterials? ACS Infect Dis 6:168-172.

511 10. Houghton JL, Green KD, Chen W, Garneau-Tsodikova S. 2010. The future of
512 aminoglycosides: the end or renaissance? Chembiochem 11:880-902.

513 11. Ramirez MS, Tolmasky ME. 2017. Amikacin: uses, resistance, and prospects for inhibition.
514 Molecules 22.

515 12. Vakulenko SB, Mobashery S. 2003. Versatility of aminoglycosides and prospects for their
516 future. Clin Microbiol Rev 16:430-50.

517 13. Ramirez MS, Nikolaidis N, Tolmasky ME. 2013. Rise and dissemination of aminoglycoside
518 resistance: the *aac(6')-Ib* paradigm. Front Microbiol 4:121.

519 14. Tolmasky ME. 2007. Aminoglycoside-modifying enzymes: characteristics, localization, and
520 dissemination., p 35-52. *In* Tolmasky ME, Bonomo RA (ed), Enzyme-Mediated Resistance

521 to Antibiotics: Mechanisms, Dissemination, and Prospects for Inhibition. ASM Press,
522 Washington, DC.

523 15. Reyes-Lamothe R, Tran T, Meas D, Lee L, Li AM, Sherratt DJ, Tolmasky ME. 2014. High-copy
524 bacterial plasmids diffuse in the nucleoid-free space, replicate stochastically and are
525 randomly partitioned at cell division. Nucleic Acids Res 42:1042-51.

526 16. Maurice F, Broutin I, Podglajen I, Benas P, Collatz E, Dardel F. 2008. Enzyme structural
527 plasticity and the emergence of broad-spectrum antibiotic resistance. EMBO Rep 9:344-
528 9.

529 17. Vetting MW, Park CH, Hegde SS, Jacoby GA, Hooper DC, Blanchard JS. 2008. Mechanistic
530 and structural analysis of aminoglycoside *N*-acetyltransferase AAC(6')-Ib and its
531 bifunctional, fluoroquinolone-active AAC(6')-Ib-cr variant. Biochemistry 47:9825-35.

532 18. Chavideh R, Sholly S, Panaite D, Tolmasky ME. 1999. Effects of F171 mutations in the 6'-N-
533 acetyltransferase type Ib [AAC(6')-Ib] enzyme on susceptibility to aminoglycosides.
534 Antimicrob Agents Chemother 43:2811-2.

535 19. Panaite DM, Tolmasky ME. 1998. Characterization of mutants of the 6'-*N*-acetyltransferase
536 encoded by the multiresistance transposon Tn*1331*: effect of Phen171-to-Leu171 and
537 Tyr80-to-Cys80 substitutions. Plasmid 39:123-33.

538 20. Shmara A, Weinsetel N, Dery KJ, Chavideh R, Tolmasky ME. 2001. Systematic analysis of a
539 conserved region of the aminoglycoside 6'-*N*-acetyltransferase type Ib. Antimicrob Agents
540 Chemother 45:3287-92.

541 21. Cook LC, Dunny GM. 2013. Effects of biofilm growth on plasmid copy number and
542 expression of antibiotic resistance genes in *Enterococcus faecalis*. Antimicrob Agents
543 Chemother 57:1850-6.

544 22. Sandegren L, Andersson DI. 2009. Bacterial gene amplification: implications for the
545 evolution of antibiotic resistance. Nat Rev Microbiol 7:578-88.

546 23. Tolmasky ME, Chamorro RM, Crosa JH, Marini PM. 1988. Transposon-mediated amikacin
547 resistance in *Klebsiella pneumoniae*. Antimicrob Agents Chemother 32:1416-20.

548 24. Edlund T, Normark S. 1981. Recombination between short DNA homologies causes
549 tandem duplication. Nature 292:269-71.

550 25. Nordstrom K, Ingram LC, Lundback A. 1972. Mutations in R factors of *Escherichia coli*
551 causing an increased number of R-factor copies per chromosome. J Bacteriol 110:562-9.

552 26. Peterson BC, Rownd RH. 1985. Drug resistance gene amplification of plasmid NR1
553 derivatives with various amounts of resistance determinant DNA. J Bacteriol 161:1042-8.

554 27. Roth JR. 2011. The joys and terrors of fast adaptation: new findings elucidate antibiotic
555 resistance and natural selection. Mol Microbiol 79:279-82.

556 28. Qi LS, Larson MH, Gilbert LA, Doudna JA, Weissman JS, Arkin AP, Lim WA. 2013.
557 Repurposing CRISPR as an RNA-guided platform for sequence-specific control of gene
558 expression. Cell 152:1173-83.

559 29. Bikard D, Jiang W, Samai P, Hochschild A, Zhang F, Marraffini LA. 2013. Programmable
560 repression and activation of bacterial gene expression using an engineered CRISPR-Cas
561 system. Nucleic Acids Res 41:7429-37.

562 30. Vigouroux A, Oldewurtel E, Cui L, Bikard D, van Teeffelen S. 2018. Tuning dCas9's ability to
563 block transcription enables robust, noiseless knockdown of bacterial genes. Mol Syst Biol
564 14:e7899.

565 31. Sarno R, McGillivary G, Sherratt DJ, Actis LA, Tolmasky ME. 2002. Complete nucleotide
566 sequence of *Klebsiella pneumoniae* multiresistance plasmid pJHCMW1. Antimicrob
567 Agents Chemother 46:3422-7.

568 32. EuropeanCommitteeonAntimicrobialSusceptibilityTesting. 2023. Breakpoint tables for
569 interpretation of MICs and zone diameters, Version 13.1. https://www.eucast.org.
570 Accessed

571 33. Beattie TR, Kapadia N, Nicolas E, Uphoff S, Wollman AJ, Leake MC, Reyes-Lamothe R. 2017.
572 Frequent exchange of the DNA polymerase during bacterial chromosome replication. Elife
573 6:e21763.

574 34. McEvoy AL, Hoi H, Bates M, Platonova E, Cranfill PJ, Baird MA, Davidson MW, Ewers H,
575 Liphardt J, Campbell RE. 2012. mMaple: a photoconvertible fluorescent protein for use in
576 multiple imaging modalities. PLoS One 7:e51314.

577 35. Soler Bistue AJ, Martin FA, Petroni A, Faccone D, Galas M, Tolmasky ME, Zorreguieta A.
578 2006. *Vibrio cholerae* InV117, a class 1 integron harboring *aac(6')-Ib* and *bla*CTX-M-2, is
579 linked to transposition genes. Antimicrob Agents Chemother 50:1903-7.

580 36. Tolmasky ME. 1990. Sequencing and expression of *aadA*, *bla*, and *tnpR* from the
581 multiresistance transposon Tn*1331*. Plasmid 24:218-26.

582 37. Takamura Y, Nomura G. 1988. Changes in the intracellular concentration of acetyl-CoA and
583 malonyl-CoA in relation to the carbon and energy metabolism of E*scherichia coli* K12. J
584 Gen Microbiol 134:2249-53.

585 38. Minsky A, Summers RG, Knowles JR. 1986. Secretion of beta-lactamase into the periplasm
586 of *Escherichia coli*: evidence for a distinct release step associated with a conformational
587 change. Proc Natl Acad Sci U S A 83:4180-4.

588 39. Dery KJ, Soballe B, Witherspoon MS, Bui D, Koch R, Sherratt DJ, Tolmasky ME. 2003. The
589 aminoglycoside 6'-*N*-acetyltransferase type Ib encoded by Tn*1331* is evenly distributed
590 within the cell's cytoplasm. Antimicrob Agents Chemother 47:2897-902.

591 40. Diederich L, Rasmussen LJ, Messer W. 1992. New cloning vectors for integration in the
592 lambda attachment site *attB* of the *Escherichia coli* chromosome. Plasmid 28:14-24.

593 41. Geu-Flores F, Nour-Eldin HH, Nielsen MT, Halkier BA. 2007. USER fusion: a rapid and
594 efficient method for simultaneous fusion and cloning of multiple PCR products. Nucleic
595 Acids Res 35:e55.

596 42. Tinevez JY, Perry N, Schindelin J, Hoopes GM, Reynolds GD, Laplantine E, Bednarek SY,
597 Shorte SL, Eliceiri KW. 2017. TrackMate: An open and extensible platform for single-
598 particle tracking. Methods 115:80-90.

599 43. Uphoff S, Reyes-Lamothe R, Garza de Leon F, Sherratt DJ, Kapanidis AN. 2013. Single-
600 molecule DNA repair in live bacteria. Proc Natl Acad Sci U S A 110:8063-8.

601 44. Dewitt SK, Adelberg EA. 1962. The occurrence of a genetic transposition in a strain of
602 *Escherichia coli*. Genetics 47:577-85.

603 45. Wood WB. 1966. Host specificity of DNA produced by *Escherichia coli*: bacterial mutations
604 affecting the restriction and modification of DNA. J Mol Biol 16:118-33.

605 46. Soubry N, Wang A, Reyes-Lamothe R. 2019. Replisome activity slowdown after exposure
606 to ultraviolet light in Escherichia coli. Proc Natl Acad Sci U S A 116:11747-11753.

607